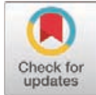

Optical Materials EXPRESS

Effect of rapid thermal annealing on the optical properties of GaAsSb alloys

XIAN GAO,[1] ZHIPENG WEI,[1,3] XUAN FANG,[1] JILONG TANG,[1] DAN FANG,[1] DENGKUI WANG,[1] XUEYING CHU,[1] JINHUA LI,[1] XIAOHUI MA,[1] XIAOHUA WANG,[1] AND RUI CHEN[2,4]

[1]*State Key Laboratory of High Power Semiconductor Laser, School of Science, Changchun University of Science and Technology, 7089 Wei-Xing Road, Changchun 130022, China*
[2]*Department of Electrical and Electronic Engineering, South University of Science and Technology of China, Shenzhen, Guangdong 518055, China*
[3]*zpweicust@126.com*
[4]*chen.r@sustc.edu.cn*

Abstract: GaAsSb ternary alloys are fundamental components of advanced electronic and optoelectronic devices in the future. The presence of localized states could greatly affect the optical properties in GaAsSb alloy, which depend on the fluctuation of alloy composition. In order to optimize the optical properties, GaAsSb alloys were treated by rapid thermal annealing (RTA) at different temperatures, and the optical behaviors of the annealed samples were investigated in detail. During RTA, a significant reduction of the localized states was observed by photoluminescence (PL) spectral analysis. Furthermore, the RTA process also altered the distribution of the components of the GaAsSb alloy, which caused a slight red-shift of the maximum PL peak at 150 K. The relationship between the localized states and the temperature of the RTA process was also investigated. The process involving the conversion of localized carriers to free carriers was proposed. Under the suitable RTA conditions, the Sb component was homogenized and the depth of carrier localization was decreased.

© 2017 Optical Society of America

OCIS codes: (160.0160) Materials; (250.0250) Optoelectronics.

Reference and links

1. T. Shi, H. E. Jackson, L. M. Smith, N. Jiang, Q. Gao, H. H. Tan, C. Jagadish, C. Zheng, and J. Etheridge, "Emergence of localized states in narrow GaAs/AlGaAs nanowire quantum well tubes," Nano Lett. **15**(3), 1876–1882 (2015).
2. M. Heiss, Y. Fontana, A. Gustafsson, G. Wüst, C. Magen, D. D. O'Regan, J. W. Luo, B. Ketterer, S. Conesa-Boj, A. V. Kuhlmann, J. Houel, E. Russo-Averchi, J. R. Morante, M. Cantoni, N. Marzari, J. Arbiol, A. Zunger, R. J. Warburton, and A. Fontcuberta i Morral, "Self-assembled quantum dots in a nanowire system for quantum photonics," Nat. Mater. **12**(5), 439–444 (2013).
3. L. Ma, W. Hu, Q. Zhang, P. Ren, X. Zhuang, H. Zhou, J. Xu, H. Li, Z. Shan, X. Wang, L. Liao, H. Q. Xu, and A. Pan, "Room-temperature near-infrared photodetectors based on single heterojunction nanowires," Nano Lett. **14**(2), 694–698 (2014).
4. J. Kim, J. Hwang, K. Song, N. Kimet, J. C. Shin, and J. Lee, "Ultra-thin flexible GaAs photovoltaics in vertical forms printed on metal surfaces without interlayer adhesives," Appl. Phys. Lett. **108**(25), 253101 (2016).
5. O. Persson, J. L. Webb, K. A. Dick, C. Thelander, A. Mikkelsen, and R. Timm, "Scanning Tunneling Spectroscopy on InAs-GaSb Esaki Diode Nanowire Devices during Operation," Nano Lett. **15**(6), 3684–3691 (2015).
6. B. M. Borg, K. A. Dick, B. Ganjipour, M. E. Pistol, L. E. Wernersson, and C. Thelander, "InAs/GaSb heterostructure nanowires for tunnel field-effect transistors," Nano Lett. **10**(10), 4080–4085 (2010).
7. Y. Sun, L. Yuan, X. Wu, Y. Cong, K. Huang, and S. Feng, "Infrared absorption enhancement by charge transfer in Ga-GaSb metal-semiconductor nanohybrids," Langmuir **32**(17), 4189–4193 (2016).
8. W. S. Liu, H. L. Tseng, and P. C. Kuo, "Enhancing optical characteristics of InAs/InGaAsSb quantum dot structures with long-excited state emission at 1.31 μm," Opt. Express **22**(16), 18860–18869 (2014).
9. F. Mezrag, N. Y. Aouina, and N. Bouarissa, "Optoelectronic and dielectric properties of $GaAs_xSb_{1-x}$ ternary alloys," J. Mater. Sci. **41**(16), 5323–5328 (2006).
10. K. A. Dao, D. K. Dao, T. D. Nguyen, A. T. Phan, and H. M. Do, "The effects of Au surface diffusion to fomation of Au droplets/clusters and nanowire growth on GaAs substrate using VLS method," J. Mater. Sci. Mater. Electron. **23**(11), 2065–2074 (2012).

#274513 https://doi.org/10.1364/OME.7.001971
Journal © 2017 Received 26 Aug 2016; revised 8 Nov 2016; accepted 9 Nov 2016; published 17 May 2017

11. X. D. Luo, C. Y. Hu, Z. Y. Xu, H. L. Luo, Y. Q. Wang, J. N. Wang, and W. K. Ge, “Selectively excited photoluminescence of $GaAs_{1−x}Sb_x$/GaAs single quantum wells,” Appl. Phys. Lett. **81**(20), 3795–3797 (2002).
12. Y. S. Chiu, M. H. Ya, W. S. Su, and Y. F. Chen, “Properties of photoluminescence in type-II GaAsSb/GaAs multiple quantum wells,” J. Appl. Phys. **92**(10), 5810–5813 (2002).
13. R. Kudrawiec, G. Sek, K. Ryczko, J. Misiewicz, and J. C. Harmand, “Photoreflectance investigations of oscillator strength and broadening of optical transitions for GaAsSb-GaInAs/GaAs bilayer quantum wells,” Appl. Phys. Lett. **84**(18), 3453–3455 (2004).
14. L. Ma, X. Zhang, H. Li, H. Tan, Y. Yang, Y. Xu, W. Hu, X. Zhu, X. Zhuang, and A. Pan, “Bandgap-engineered GaAsSb alloy nanowires for near-infrared photodetection at 1.31 μm,” Semicond. Sci. Technol. **30**(10), 105033 (2015).
15. Z. Li, X. Yuan, L. Fu, K. Peng, F. Wang, X. Fu, P. Caroff, T. P. White, H. Hoe Tan, and C. Jagadish, “Room temperature GaAsSb single nanowire infrared photodetectors,” Nanotechnology **26**(44), 445202 (2015).
16. J. Huh, H. Yun, D. C. Kim, A. M. Munshi, D. L. Dheeraj, H. Kauko, A. T. J. van Helvoort, S. Lee, B. O. Fimland, and H. Weman, “Rectifying single GaAsSb nanowire devices based on self-induced compositional gradients,” Nano Lett. **15**(6), 3709–3715 (2015).
17. D. Ren, D. L. Dheeraj, C. Jin, J. S. Nilsen, J. Huh, J. F. Reinertsen, A. M. Munshi, A. Gustafsson, A. T. J. van Helvoort, H. Weman, and B. O. Fimland, “New insights into the origins of Sb-induced effects on self-catalyzed GaAsSb nanowire arrays,” Nano Lett. **16**(2), 1201–1209 (2016).
18. H. Detz, A. M. Andrews, M. Nobile, P. Klang, E. Mujagić, G. Hesser, W. Schrenk, F. Schäffler, and G. Strasser, “Intersubband optoelectronics in the InGaAs/GaAsSb material system,” J. Vac. Sci. Technol. B **28**(3), C3G19, G23 (2010).
19. X. Gao, Z. Wei, F. Zhao, Y. Yang, R. Chen, X. Fang, J. Tang, D. Fang, D. Wang, R. Li, X. Ge, X. Ma, and X. Wang, “Investigation of localized states in GaAsSb epilayers grown by molecular beam epitaxy,” Sci. Rep. **6**, 29112 (2016).
20. Y. Gao, H. Liu, R. Shi, N. Zhou, Z. Xu, Y. M. Zhu, J. F. Nie, and Y. Wang, “Simulation study of precipitation in an Mg-Y-Nd alloy,” Acta Mater. **60**(12), 4819–4832 (2012).
21. Y. Gao, N. Zhou, F. Yang, Y. Cui, L. Kovarik, N. Hatcher, R. Noebe, M. J. Mills, and Y. Wang, “P-phase precipitation and its effect on martensitic transformation in (Ni, Pt) Ti shape memory alloys,” Acta Mater. **60**(4), 1514–1527 (2012).
22. X. D. Luo, P. H. Tan, Z. Y. Xu, and W. K. Ge, “Selectively excited photoluminescence of $GaAs_{1-x}N_x$ single quantum wells,” J. Appl. Phys. **94**(8), 4863–4865 (2003).
23. S. Shirakata, M. Kondow, and T. Kitatani, “Temperature-dependent photoluminescence of high-quality GaInNAs single quantum wells,” Appl. Phys. Lett. **80**(12), 2087–2089 (2002).
24. H. Zhu, C. X. Shan, B. H. Li, Z. Z. Zhang, J. Y. Zhang, B. Yao, D. Z. Shen, and X. W. Fan, “Enhanced photoluminescence caused by localized excitons observed in MgZnO alloy,” J. Appl. Phys. **105**(10), 103508 (2009).
25. X. Fang, Z. Wei, R. Chen, J. Tang, H. Zhao, L. Zhang, D. Zhao, D. Fang, J. Li, F. Fang, X. Chu, and X. Wang, “Influence of exciton localization on the emission and ultraviolet photoresponse of ZnO/ZnS core-shell nanowires,” ACS Appl. Mater. Interfaces **7**(19), 10331–10336 (2015).
26. X. Fang, Z. Wei, Y. Yang, R. Chen, Y. Li, J. Tang, D. Fang, H. Jia, D. Wang, J. Fan, X. Ma, B. Yao, and X. Wang, “Ultraviolet electroluminescence from ZnS@ ZnO core-shell nanowires/p-GaN introduced by exciton localization,” ACS Appl. Mater. Interfaces **8**(3), 1661–1666 (2016).
27. S. Jin, Y. Zheng, and A. Li, “Characterization of photoluminescence intensity and efficiency of free excitons in semiconductor quantum well structures,” J. Appl. Phys. **82**(8), 3870–3873 (1997).
28. J. A. Van Vechten and T. K. Bergstresser, “Electronic structures of semiconductor alloys,” Phys. Rev. B **1**(8), 3351–3358 (1970).
29. M. Aziz, J. F. Felix, D. Jameel, N. A. Saqri, F. S. A. Mashary, H. M. Alghamdi, H. M. A. Albalawi, D. Taylor, and M. Henini, “Rapid thermal annealing: An efficient method to improve the electrical properties of tellurium compensated Interfacial Misfit GaSb/GaAs heterostructures,” Superlattices Microstruct. **88**, 80–89 (2015).
30. R. Woscholski, M. K. Shakfa, S. Gies, M. Wiemer, A. Rahimi-Iman, M. Zimprich, S. Reinhard, K. Jandieri, S. D. Baranovskii, W. Heimbrodt, K. Volz, W. Stolz, and M. Koch, “Time-resolved photoluminescence of Ga (NAsP) multiple quantum wells grown on Si substrate: Effects of rapid thermal annealing,” Thin Solid Films **613**, 55–58 (2016).
31. O. Donmez, K. Kara, A. Erol, E. Akalin, H. Makhloufi, A. Arnoult, and C. Fontaine, “Thermal annealing effects optical and structural properties of GaBiAs epilayers: Origin of the thermal annealing-induced redshift in GaBiAs,” J. Alloys Compd. **686**, 976–981 (2016).
32. A. Jebali, N. Khemiri, and M. Kanzar, “The effect of annealing in N_2 atmosphere on the physical properties of $SnSb_4S_7$ thin films,” J. Alloys Compd. **673**, 38–46 (2016).
33. P. Fan, J. Zhao, G. Liang, D. Gu, Z. Zheng, D. Zhang, X. Cai, J. Luo, and F. Ye, “Effects of annealing treatment on the properties of CZTSe thin films deposited by RF-magnetron sputtering,” J. Alloys Compd. **625**, 171–174 (2015).
34. A. Satake, Y. Masumoto, T. Miyajima, T. Asatsuma, F. Nakamura, and M. Ikeda, “Localized exciton and its stimulated emission in surface mode from single-layer $In_xGa_{1−x}N$,” Phys. Rev. B **57**(4), R2041–R2044 (1998).
35. Y. P. Varshni, “Temperature dependence of the energy gap in semiconductors,” Physica **34**(1), 149–154 (1967).

36. S. Francoeur, S. A. Nikishin, C. Jin, Y. Qiu, and H. Temkin, "Excitons bound to nitrogen clusters in GaAsN," Appl. Phys. Lett. **75**(11), 1538–1540 (1999).
37. V. V. Chaldyshev, A. L. Kolesnikova, N. A. Bert, and A. E. Romanov, "Investigation of dislocation loops associated with As-Sb nanoclusters in GaAs," J. Appl. Phys. **97**(2), 024309 (2005).
38. D. F. Reyes, J. M. Ulloa, A. Guzman, A. Hierro, D. L. Sales, R. Beanland, A. M. Sanchez, and D. González, "Effect of annealing in the Sb and In distribution of type II GaAsSb-capped InAs quantum dots," Semicond. Sci. Technol. **30**(11), 114006 (2015).
39. D. F. Reyes, D. González, J. M. Ulloa, D. L. Sales, L. Dominguez, A. Mayoral, and A. Hierro, "Impact of N on the atomic-scale Sb distribution in quaternary GaAsSbN-capped InAs quantum dots," Nanoscale Res. Lett. **7**(1), 653 (2012).
40. S. Lee, A. Nathan, Y. Ye, Y. Guo, and J. Robertson, "Localized tail states and electron mobility in amorphous ZnON thin film transistors," Sci. Rep. **5**, 13467 (2015).

1. Introduction

Owing to their advantages in potential optoelectronic and electronic device applications [1–5], III-V semiconductors based on GaAs and GaSb materials have attracted great attention in recent years. Among them, $GaAs_xSb_{1-x}$ can be obtained by incorporating antimony (Sb) into GaAs, allowing the band gap to be easily adjusted from 0.75 to 1.42 eV [6–10]. The diversity of semiconductor structures had been developed, such as GaAsSb/GaAs single/multiple quantum wells [11, 12], GaAsSb-GaInAs/GaAs bilayer quantum wells [13], and GaAsSb nanowires [14–17]. GaAsSb was recognized as the important material for fabrication high-performance optoelectronic devices, such as laser diodes, photo-detectors and transistors [5, 17, 18]. However, the component fluctuations in ternary alloys could cause the localized states in these materials [1, 19–21], resulting in carrier localization effect. The carrier localization effect could greatly affect the optical properties of the semiconductors. The emission efficiency could be influenced by localized carriers in semiconductor materials, such as GaAsSb, InGaN, GaAsN and MgZnO [19, 22–24]. In addition, the optoelectronic performance of devices can also be tuned by manipulating localized states [25, 26]. Although the crystal quality and compositional uniformity of these materials could be improved by optimization of the growth conditions, the carrier localization effect was still an unsolved issue. Therefore, a post-treatment was needed to manipulate the localized carriers in semiconductor alloys.

Post-annealing procedures are commonly used to improve the structural and optical properties of semiconductors [27–33]. For example, rapid thermal annealing (RTA), in which the material is heated to a high temperature for a period of seconds, is beneficial for the healing of certain types of structural defects, the relaxation of residual stress, the prevention of diffusion and the improvement of the alloy uniformity. With these advantages, the RTA process could be developed as an effective method to modulating the properties of localized states. In our previous work [19], it is found that the degree of exciton localization was proportional to the Sb content of GaAsSb alloys. In the present work, the effect of RTA on the morphology and optical properties of GaAsSb alloys has been investigated in detail. The crystal and optical morphology of GaAsSb can be improved after RTA treatment. Additionally, photoluminescence (PL) measurements indicated that the optical properties of GaAsSb were closely dependent on the RTA treatment conditions. The results showed that the suitable RTA conditions promoted the homogeneous distribution of components and allowed manipulating the depth of localized states in GaAsSb alloys.

2. Experimental

A GaAsSb alloy with a thickness of 350 nm was grown on a GaAs substrate in a molecular beam epitaxy (MBE) system (DCA-P600) with a 100 nm GaAs buffer layer. Detailed growth conditions were described in our previous work [19]. The actual growth temperature was 460 ± 20 °C. The concentration of Sb in the GaAsSb epilayer was controlled via the Sb beam flux, and was about 8%. After growth of the alloy, three samples of it were treated by RTA, with a treatment time of 30 s and with annealing temperatures of 500 °C, 600 °C and 700 °C,

respectively. The annealing procedure was carried out under a nitrogen atmosphere at ambient pressure using a commercially available RTA reactor (AccuThermo AW410, Allwin21 Corp.). The morphologies of the samples were observed using a Multimode 8 Atomic Force Microscope (AFM).

The PL spectra were recorded using a HORIBA iHR550 spectrometer with an InGaAs detector. A 655 nm semiconductor diode laser was used as the excitation source. A standard phase lock-in amplification technique was employed to enhance the signal-to-noise ratio. During measurement of the temperature-dependent PL spectra, the excitation power used was 80 mW and the spot area of the laser was approximately 0.4 cm^2.

3. Results and discussion

Figure 1 shows the PL spectra of the samples at 150 K. All the samples exhibited evidence of near band-edge (NBE) emission, labeled as A, B, C and D, respectively. For the as-grown sample, the PL spectrum presented one peak (A) located at 1.364 eV with a full-width at half-maximum (FWHM) of 15 meV. For the samples annealed at 500 °C (or 600 °C, or 700 °C), the emission peaks B (or C, or D) were observed at 1.35 eV (or 1.344 eV, or 1.338 eV) with a FWHM of 17 meV (or 23 meV, or 21 meV). As the annealing temperature increased, the PL peak positions showed a slight red-shift of 14-26 meV, indicating that the band gaps of the samples had decreased. According to the literature [28], changes of the band gap can have several possible causes, including compositional changes of the alloy, thermal effects or the presence of localized states. In addition to the changes of band gap, the samples showed distinct FWHM values (as shown in the inset of Fig. 1). The reasons for this will be discussed later, but for now it can be stated. To qualitatively illustrate the changes in the annealed samples, their PL spectra with absolute intensities are displayed. The sample annealed at 500 °C present the strongest PL intensity, which implied the better optical property. Based on the PL results, the emission behavior of the alloys changed after the RTA process.

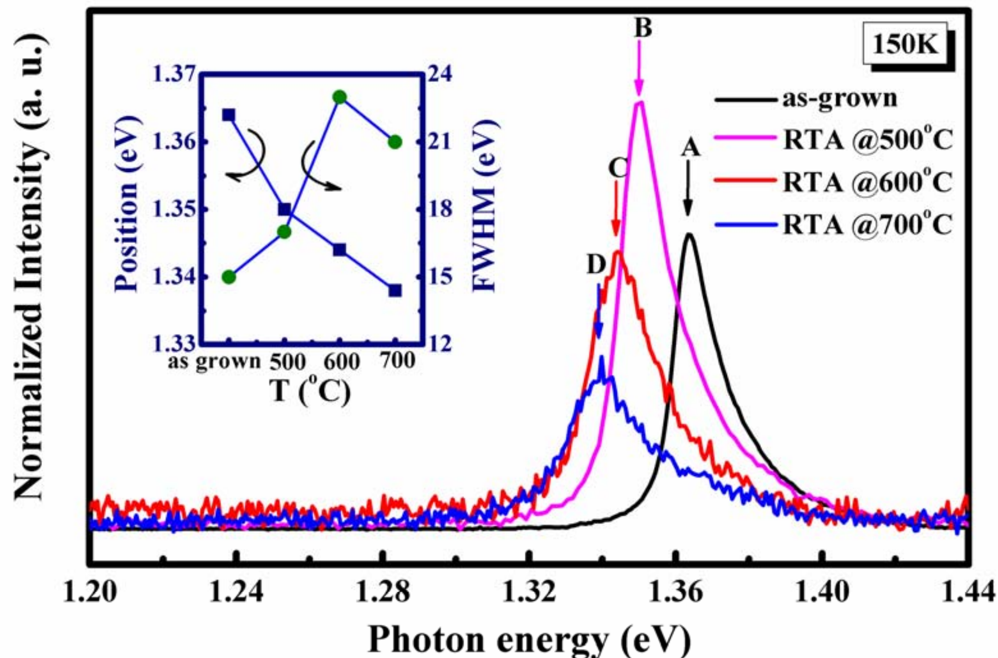

Fig. 1. PL spectra of the samples at 150 K; inset shows the changes of peak position and FWHM with different annealing temperatures.

Optical Materials EXPRESS

To investigate the electronic transition mechanism of the GaAsSb alloys after annealing, low-temperature and temperature-dependent PL measurements were carried out. Figure 2(a) displays the PL spectra of the samples at 10 K. The PL spectra could be well-fitted by two individual Gaussian peaks, labeled P_1 and P_2, for each sample, in which the emission with higher photon energy is P_1. For the as-grown sample, the P_1 and P_2 emission were the transitions corresponding to free- and localized-carrier emission (FE and LE), located at 1.391 eV and 1.379 eV, respectively [19]. For the annealed samples, the P_1 emissions were located at 1.384 eV, 1.371 eV and 1.365 eV, could be assumed to correspond to FE, while the P_2 emissions, located at 1.368 eV, 1.359 eV and 1.354 eV, could be assumed to arise from LE. Besides their different peak positions, P_1 and P_2 were also different in PL intensity, as shown in Fig. 2(b). It can be seen in Fig. 2(c) that the emission intensity of P_1 was greater than that of P_2 in the sample annealed at 500 °C, while the reverse result was true in other samples. Thus, from the low-temperature PL measurements, it was concluded that the RTA temperature influenced the relative abundance of free and localized carriers. Based on above premise, P_1 and P_2 emissions could be attributed to FE and LE, respectively. And 500 °C was the suitable annealing temperature, which could be confirmed by the result of strongest P_1 emission and the weakest P_2 emission among the three annealed samples.

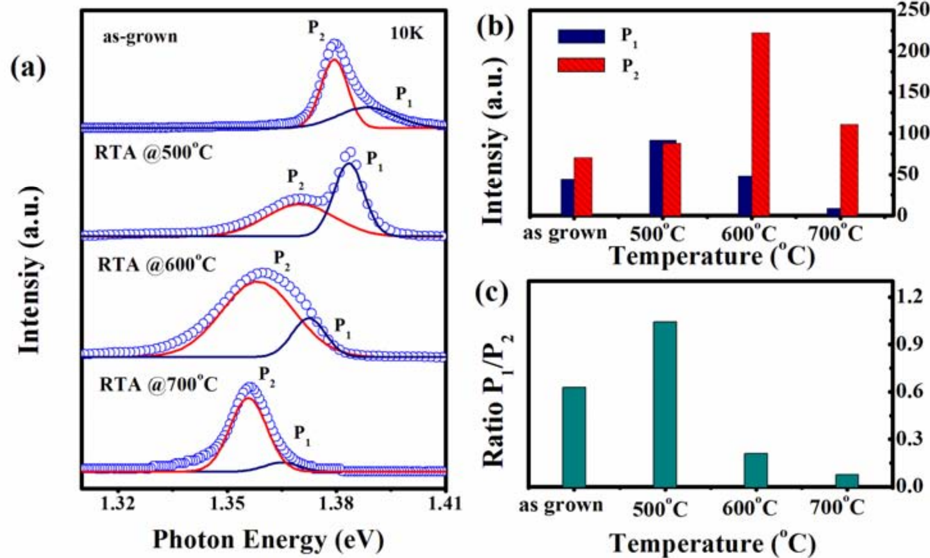

Fig. 2. (a) Gaussian-fitting results of the low-temperature PL spectra of the samples at 10 K; (b) Intensity of the P_1 and P_2 emissions in each sample; (c) Intensity ratio of P_1 to P_2 in each sample.

To further explore the origin of the P_1 (P_2) emissions and the relationship between them, temperature-dependent PL spectra from 10 K to 150 K were measured, as shown in Fig. 3. The as-grown sample was exhibited a typical behavior of emission from localized states, as shown in Fig. 3 (a). The existence of localized states could be confirmed by "S"-shaped temperature-dependent PL emission which arising from the incorporation of Sb into the GaAsSb alloy [19, 34]. Figure 3 (b) shows the temperature-dependent PL spectra of the sample annealed at 500 °C. With the temperature increasing, the photon energy of P_1 gradually red shifted, while the P_2 emission was quenched at about 30 K. Thus, when the temperature was increased to 150 K, the emission was dominated by P_1 in the sample of annealed at 500 °C. Figure 3(c) shows the temperature-dependent PL spectra of the sample annealed at 600 °C. A transition process from P_2 to P_1 was occurred in the temperature range from 10 K to 40 K, which was not obvious in the previous sample. This behavior is consistent

with the presence of localized states (which were insensitive to temperature). The similar temperature-dependent PL spectra were found in our earlier work [25, 26]. The phenomenon could be explained by the carriers escaped from localized states and conversion into free carriers by absorbed thermal energy. Finally, the temperature-dependent PL spectra for the sample annealed at 700 °C were shown in Fig. 3 (d). Here, another type of "S"-shaped emission pattern was observed, together with a transition process from P_2 to P_1. However, the transition occurred in the temperature range from 40 K to 80 K in this case. Figure 4 shows the power-dependent PL spectra of the sample annealed at 700 °C, and the PL intensity exhibited an approximately linear relationship with increasing excitation power. The relationship between the integrated PL emission intensity and excitation power can be fitted by the expression $I_{PL} \propto I_{EX}^{\alpha}$ (as shown in the inset of Fig. 4). The radiative recombination mechanism could be deduced from the value of the parameter α. In this case, α was about 1.33, which was indicated that the emission was related to excitonic recombination [27]. The blue-shift of the emission indicated that the population of localized carriers was gradually saturated with the excitation power increasing, resulting in their conversion to free carriers. Therefore, the P_1 and P_2 emissions could be ascribed to FE and LE, respectively.

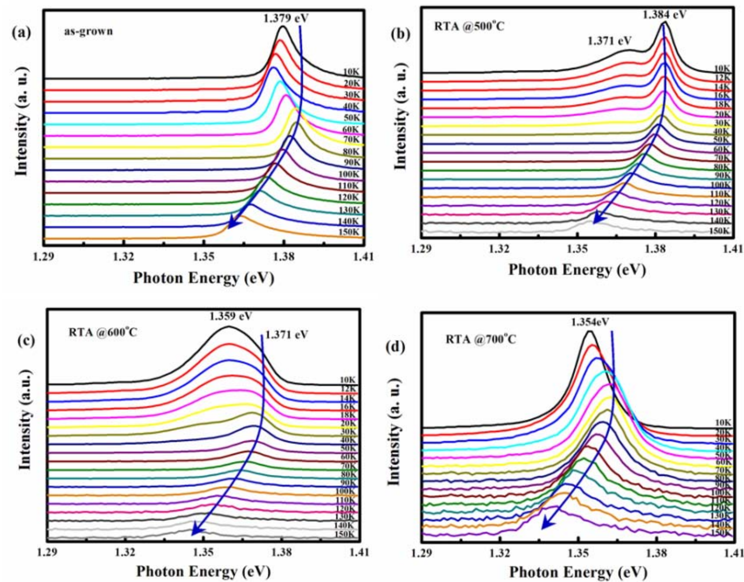

Fig. 3. Temperature-dependent PLspectra of the samples.

Based on the temperature-dependent PL spectra, it is evident that the RTA temperature affected the FE and LE emission properties of the samples. Figure 5 shows the photon energies of the emission peaks of P_1 and P_2 as a function of temperature for the as-grown and annealed samples. At higher temperatures, the photon energies of the free excitons can be well fitted by the Varshni empirical equation: $E_g = E_0 - \alpha T^2 / (T + \beta)$ [35]. However, in the range of low temperatures, the photon energies of the emissions could not be fitted well because of the existence of localized states. The energy separation between P_1 and P_2, denoted by ΔE, represented the degree of carrier localization. The ΔE values of the as-grown sample and those annealed at 500 °C, 600 °C and 700 °C were 14.8 meV, 7.9 meV, 12.9 meV and 15.2 meV, respectively (as shown in Fig. 5). Additionally, the temperature, denoted by ΔT, indicated the temperature localized excitons were converted into free excitons, was also found different among the samples, and values of ΔT were 70 K, 30 K, 40 K and 80 K, respectively.

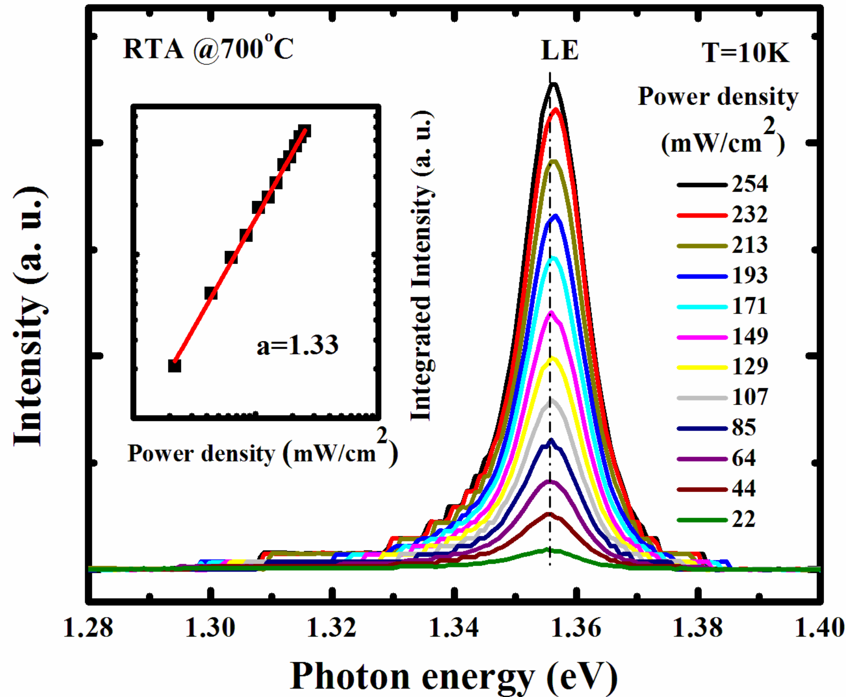

Fig. 4. Low-temperature (10 K) power-dependent PL spectra of GaAsSb sample annealed at 700 °C.

It is known that atom clusters could cause nonuniform component inside alloy, such as hierarchical complexes in GaAsN alloys [36]. In the as-grown GaAsSb alloys, the incorporation of Sb could form Sb cluster, which could lead to the formation of localized states [1, 19, 30]. The PL emission related to FE and LE also supports this claim. However, the migration of N or Sb clusters inside the alloys could be realized by annealing [36–39]. Therefore, it can be considered that the alloy uniformity could be improved by using optimal annealing temperature, and localization potential also could be decreased. At higher-than-optimal annealing temperatures, the degree of migration will increasing, and defects (such as loop dislocations) or Sb-rich clusters would be re-formed [38, 39]. Eventually, the new population of localized states will be formed. From the AFM images of the samples (the insets of Fig. 5), their surface roughnesses (measured as the root mean square, RMS) can be calculated as 1.218 nm, 1.06 nm, 1.515 nm and 1.599 nm, respectively. The surface area difference of the samples changed from 0.00792% to 0.0206%. The AFM results provide the secondary evidence of the degree of Sb migration, and the changes in surface roughness imply the formation and disappearance of localized states as the annealing temperature was increased.

Figure 6 is a schematic illustration explaining the relationship between FE and LE. The as-grown sample and annealed samples contained localized states with a certain value of ΔE ($\Delta E_{as\text{-}grown}$, $\Delta E_{500°C}$, $\Delta E_{600°C}$, $\Delta E_{700°C}$, respectively). Free carriers were trapped by localized states and converted into localized carriers in these samples. And the localized carriers also could be released from the localized states by absorbing thermal energy, and became free carriers again [40]. However, it is worth to note that the RTA process could induce the migration of Sb and the alloy composition was under the influence of this migration [38, 39]. Furthermore, the degree of carrier localization was also changed. The optimal RTA temperature, i.e., the sample of annealed at 500 °C, had the effect of homogenizing the Sb content in the annealed sample, thus decreasing the depth of the potential fluctuations

($\Delta E_{500°C}$ <$\Delta E_{as\text{-}grown}$). In this way, the annealing temperature affected the degree of carrier localization and the optical properties of the samples.

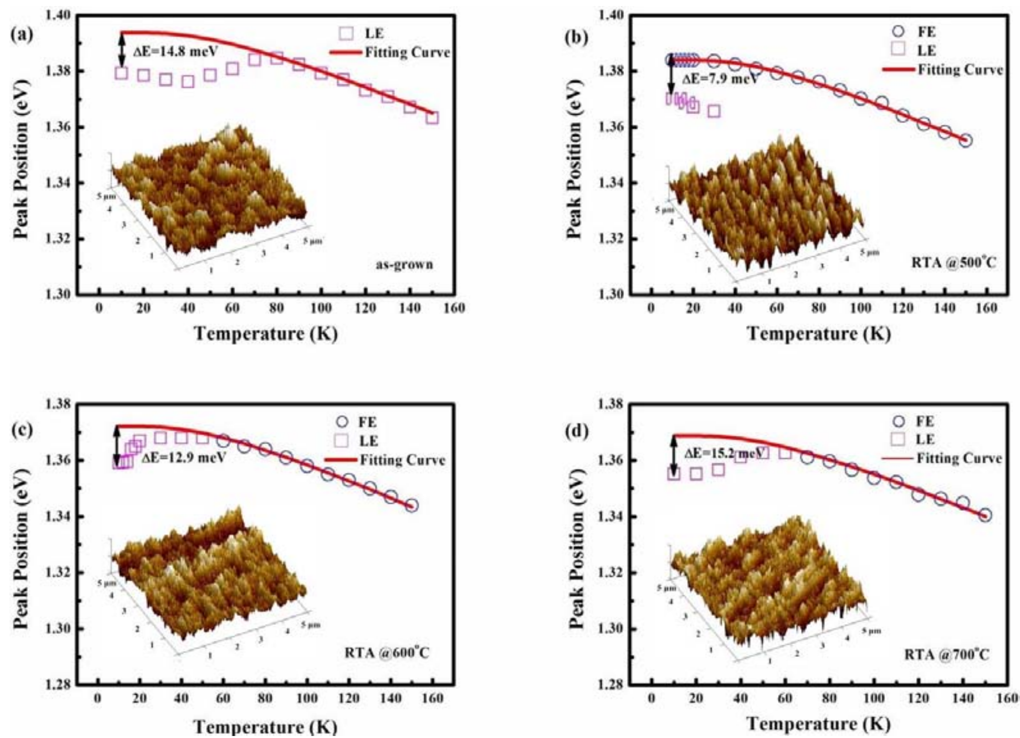

Fig. 5. Photon energy of the emission peaks of the samples with increasing temperature. The insets are the AFM images of the samples.

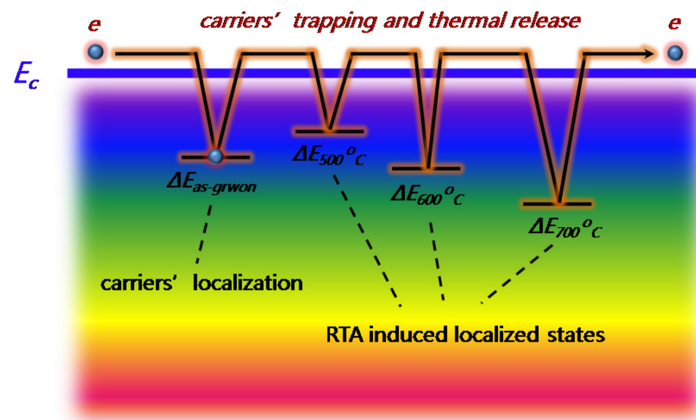

Fig. 6. Schematic illustration showing the transition processes of carriers between different localized states and the free-carrier state.

4. Conclusion

GaAsSb alloys were grown on a GaAs substrate by MBE, and were then treated by RTA at various temperatures between 500 °C and 700 °C in this research. The optical properties of the samples were investigated systemically. It is worth to note that the formation of localized states was found, and related to Sb cluster inside the GaAsSb alloy which was influenced by

the RTA temperature. The suitable RTA temperature (500 °C) beneficially reduced the density of localized defects, as well as reducing the depth of the localized states, thus enhancing the crystal quality of the GaAsSb alloy. However, higher temperatures induced the Sb-rich clusters were formed again, which could re-introduce a greater density of localized defects, and the depth of these localized states increased. These results indicate that the RTA process could be used to improve the degree of alloy disorder, such as nonuniform component. Therefore, RTA process should be recognized as an effective method to manipulate the formation and depth of localized states to improve the performance of GaAsSb-based materials and devices.

Funding

National Natural Science Foundation of China (61307045, 61404009, 61474010, 61574022, 61504012, 61674021, 11404219, 11404161, 11574130 and 11674038); Foundation of State Key Laboratory of High Power Semiconductor Lasers; Developing Project of Science and Technology of Jilin Province (20160519007JH, 20160101255JC, 20160520117JH); Project of Jilin Province Development and Reform (2014Y110); Project of Changchun Science and Technology (14 KG018); National 1000 plan for Young Talents and Shenzhen Science and Technology Innovation Committee (Projects Nos.: JCYJ20150630162649956, JCYJ20150930160634263 and KQTD2015071710313656).